

Critical endline of the finite temperature phase transition for 2+1 flavor QCD around the SU(3)-flavor symmetric point

Yoshinobu Kuramashi,^{1,2,3} Yoshifumi Nakamura,^{3,4,*} Shinji Takeda,^{5,3,†} and Akira Ukawa³

¹*Faculty of Pure and Applied Sciences, University of Tsukuba, Tsukuba, Ibaraki 305-8571, Japan*

²*Center for Computational Sciences, University of Tsukuba, Tsukuba, Ibaraki 305-8577, Japan*

³*RIKEN Advanced Institute for Computational Science, Kobe, Hyogo 650-0047, Japan*

⁴*Graduate School of System Informatics, Department of Computational Sciences, Kobe University, Kobe, Hyogo 657-8501, Japan*

⁵*Institute of Physics, Kanazawa University, Kanazawa 920-1192, Japan*

(Dated: March 4, 2022)

We investigate the critical endline of the finite temperature phase transition of QCD around the SU(3)-flavor symmetric point at zero chemical potential. We employ the renormalization-group improved Iwasaki gauge action and non-perturbatively $O(a)$ -improved Wilson-clover fermion action. The critical endline is determined by using the intersection point of kurtosis, employing the multi-parameter, multi-ensemble reweighting method to calculate observables off the SU(3)-symmetric point, at the temporal size $N_T=6$ and lattice spacing as low as $a \approx 0.19$ fm. We confirm that the slope of the critical endline takes the value of -2 , and find that the second derivative is positive, at the SU(3)-flavor symmetric point on the Columbia plot parametrized with the strange quark mass m_s and degenerated up-down quark mass m_l .

PACS numbers: 11.15.Ha,12.38.Gc

arXiv:1605.04659v1 [hep-lat] 16 May 2016

* nakamura@riken.jp

† takeda@hep.s.kanazawa-u.ac.jp

I. INTRODUCTION

The Columbia phase diagram plot [1] provides a visualization of the finite-temperature phases of 2+1 flavor QCD at zero chemical potential in the plane of the light quark mass and strange quark mass (m_l, m_s). In the small quark mass region, it is believed that the transition is of first order [2], which turns into a region of crossover as quark masses are increased. The boundary which separates the two regions is the critical endline (CEL) which belongs to the Z_2 universality class [3].

There is a longstanding issue that the results for critical endpoint (CEP) at the SU(3)-flavor symmetric point (m^{sym}) obtained by Wilson type and staggered type fermion actions are inconsistent [4–10]. Recently, we have investigated CEP with degenerate $N_f = 3$ dynamical flavors of non-perturbatively $O(a)$ -improved Wilson fermion action, and determined its location by the intersection points of kurtosis for the temporal sizes $N_T = 4, 6$ and 8 [11]. The continuum extrapolation implies a non-zero value $m_{\text{PS,CEP}} \approx 300$ MeV for the pseudoscalar meson mass. Scaling violations are large, however, necessitating further studies at larger N_T to obtain conclusive results for CEP.

In this article, we explore the properties of CEL away from m^{sym} . In particular we ask how CEL curve away from m^{sym} . This is a first step to obtain a comprehensive view on the relation of CEL and the physical point for which the strange quark mass is significantly heavier than the degenerate up-down quark mass. To set the stage for our analysis, let us consider the kurtosis $K_{\mathcal{O}}$ of some quantity \mathcal{O} which can be either a gluonic or quark quantity. The kurtosis generally depends on the quark masses m_u, m_d, m_s , and its Taylor expansion around m^{sym} will have a form $K_{\mathcal{O}} = K_0 + (\delta m_u + \delta m_d + \delta m_s)K_1 + O(\delta m^2)$ where $\delta m_q (q = u, d, s)$ denotes the difference from the SU(3)-symmetric value m^{sym} . Therefore, if one varies the quark masses while keeping the average over the three quark masses, *i.e.*, $\delta m_u + \delta m_d + \delta m_s = 0$, the kurtosis remains unchanged up to second order in the variation of the quark masses. For degenerate up and down quark mass, we have $\delta m_l = \delta m_u = \delta m_d$, and hence the change becomes

$$\delta m_s = -2\delta m_l. \quad (1)$$

This means that the slope of CEL at m^{sym} should take the value -2 on the Columbia plot.

There are no such constraints on the second derivative of CEL with respect to m_l at m^{sym} . If it is positive, CEL would smoothly curve up to the tricritical point $m_s = m_s^{\text{tric}}$ located on the axis for the strange quark mass around which CEL is expected to behave as $m_s - m_s^{\text{tric}} \sim m_l^{2/5}$ [12]. So far, a lattice QCD result obtained by using staggered fermions at $N_T = 4$ with a lattice spacing $a \approx 0.3$ fm supports such a curve [10].

This paper is organized as follows. In Section II we present the simulation details including the parameters and the simulation algorithm. Our numerical results are presented in Section III. In Section IV, we provide a brief conclusion.

II. SIMULATION DETAILS

To determine CEL away from CEP, we perform kurtosis intersection analysis using a multi-parameter, multi-ensemble reweighting method. The details of this method is described in Refs. [11, 13].

Calculations are made at a temporal lattice size $N_T = 6$ and the spacial sizes $N_L = 10, 12, 16$ and 24 with $N_f = 3$ degenerate flavors of dynamical quarks using the Iwasaki gluon action [14] and the non-perturbatively $O(a)$ -improved Wilson fermion action [15]. All observables for $N_f = 2 + 1$ QCD are computed by using a κ reweighting. The periodic boundary condition is imposed for gluon fields while the anti-periodic boundary condition is employed for quark fields. We use a highly optimized HMC code [16], applying mass preconditioning [17] and RHMC [18], 2nd order minimum norm integration scheme [19], putting the pseudo fermion action on multiple time scales [20] and a minimum residual chronological method [21] to choose the starting guess for the solver. We generate 63 ensembles of $O(100,000)$ trajectories on HA-PACS and COMA at University of Tsukuba, System E at Kyoto University and PRIMERGY CX400 tatara at Kyushu University. Measurements are done at every 10th trajectory and statistical errors are estimated by the jackknife method with the bin size of $O(1,000)$ configurations. In Table I, we summarize the simulation parameters and statistics.

In this study, we use the susceptibility, χ , of the quark condensate to determine the transition point, and its kurtosis, K , for intersection analysis to locate CEL. The quark condensate, Σ , and skewness, S , are used to check that the

TABLE I. Simulation parameters and statistics.

β	κ	# of conf.			
		$N_L = 10$	$N_L = 12$	$N_L = 16$	$N_L = 24$
1.715	0.140900	7300	4200		
1.715	0.140920	8000	3800		
1.715	0.140940	8000	8600	7900	
1.715	0.140950	8100	7900	8000	
1.715	0.140960	9500	8800	7900	
1.715	0.140970	9400	6900	8400	
1.715	0.140980	9699	6800	8800	
1.715	0.140990	9500	6300	8599	
1.715	0.141000	10000	8700	9400	
1.715	0.141010	8800	8500	8300	
1.715	0.141020	8700	8900	8600	
1.715	0.141100	8600			
1.73	0.140420	7900	7900	8900	5250
1.73	0.140430	7900	7900	8900	5100
1.73	0.140440	7900	7900	8900	5200
1.73	0.140450	8600	7900	7300	4900
1.75	0.139620	12200	10450	10100	
1.75	0.139640	12900	10400	10100	
1.75	0.139660	11700	10450	10100	
1.75	0.139680	12900	10400	9700	
1.75	0.139700	8378	4900	10100	

transition point is determined appropriately. The quantities Σ , χ , S and K are defined by

$$\begin{aligned}
\Sigma &= \frac{\langle Q_1 \rangle}{N_L^3 N_T}, \\
\chi &= \frac{\langle Q_2 \rangle - \langle Q_1 \rangle^2}{N_L^3 N_T}, \\
S &= \frac{\langle Q_3 \rangle - 3\langle Q_2 \rangle \langle Q_1 \rangle + 2\langle Q_1 \rangle^3}{(\langle Q_2 \rangle - \langle Q_1 \rangle^2)^{3/2}}, \\
K &= \frac{\langle Q_4 \rangle - 4\langle Q_3 \rangle \langle Q_1 \rangle - 3\langle Q_2 \rangle^2 + 12\langle Q_2 \rangle \langle Q_1 \rangle^2 - 6\langle Q_1 \rangle^4}{(\langle Q_2 \rangle - \langle Q_1 \rangle^2)^2},
\end{aligned} \tag{2}$$

with

$$\begin{aligned}
Q_1 &= N_f \text{tr}[D_f^{-1}], \\
Q_2 &= -N_f \text{tr}[D_f^{-2}] + (N_f \text{tr}[D_f^{-1}])^2, \\
Q_3 &= 2N_f \text{tr}[D_f^{-3}] - 3N_f^2 \text{tr}[D_f^{-2}] \text{tr}[D_f^{-1}] + (N_f \text{tr}[D_f^{-1}])^3, \\
Q_4 &= -6N_f \text{tr}[D_f^{-4}] + 8N_f^2 \text{tr}[D_f^{-3}] \text{tr}[D_f^{-1}] + 3(N_f \text{tr}[D_f^{-2}])^2 - 6N_f \text{tr}[D_f^{-2}] (N_f \text{tr}[D_f^{-1}])^2 + (N_f \text{tr}[D_f^{-1}])^4,
\end{aligned} \tag{3}$$

where

$$D_f = \frac{1}{2\kappa_f} + \frac{i}{4} c_{\text{sw}} \sigma_{\mu\nu} F_{\mu\nu}(n) \delta_{m,n} - \frac{1}{2} \sum_{\mu=1}^4 [(1 - \gamma_\mu) U_\mu(n) \delta_{n,m+\hat{\mu}} + (1 + \gamma_\mu) U_{-\mu}(n) \delta_{n,m-\hat{\mu}}]. \tag{4}$$

There are a few choices for the quark condensate in $N_f = 2 + 1$ QCD. For example, eq. (2) for $\bar{s}s$ is defined by $\kappa_f = \kappa_s$ and $N_f = 1$. In this study, we choose $\kappa_f = \kappa_l$ and $N_f = 2$ since the signal of for $\bar{u}u + \bar{d}d$ and its higher moments turns out to be better than the others. Even if we made different choices, we expect to obtain the same results because all of such ‘‘order parameters’’ would behave equally as pure magnetization in the thermodynamic limit.

III. RESULTS

We check first the validity of the reweighting from $N_f = 3$ to $N_f = 2 + 1$. Figure 1 compares Σ , χ , S and K obtained by the reweighting of the $N_f = 3$ runs at $\beta = 1.73$ with a direct $N_f = 2 + 1$ simulation at $(\beta, N_L, \kappa_1, \kappa_s) = (1.73, 12, 0.140850, 0.139500)$ as a function of κ_1 . They are in good agreement with each other.

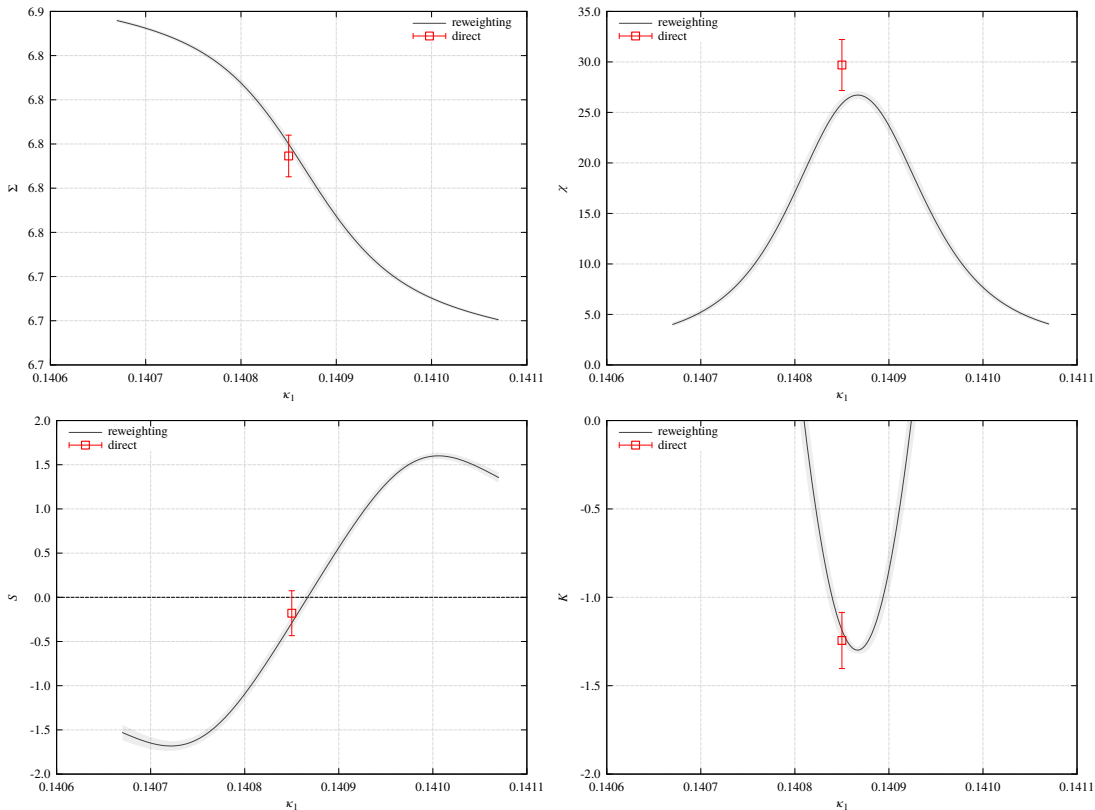


FIG. 1. Σ (left up), χ (right up), S (left bottom) and K (right bottom) as a function of κ_1 obtained by reweighting of data in Table I (curves) and those at $\beta = 1.73$, $\kappa_s = 0.13950$, $N_L = 12$ obtained by the direct simulation at $\kappa_1 = 0.140850$ (square data points).

The reweighting results for the susceptibility and kurtosis are illustrated in Fig. 2 for $\beta = 1.715$ and 1.73 and three values of κ_s as functions of κ_1 . The peak position of susceptibility gives us a very precise value of κ_1 for the transition point, and a corresponding value of kurtosis, for each β , κ_s and N_L .

Figure 3 shows the kurtosis at the transition point for three values of κ_s in Fig. 2. We fit the kurtosis at $\beta = 1.715$ and 1.73 with a finite-size scaling ansatz given by

$$K = K_E + AN_L^{1/\nu}(\beta - \beta_E), \quad (5)$$

where β_E and K_E are the values of β and K at each CEP and ν is the critical exponent along CEL. The fitting results are summarized in Table II. We find that ν and K_E are consistent with the values of the three-dimensional Z_2 universality class. The results for $\kappa_s < 0.13910$ or $\kappa_s > 0.14170$ are too noisy to determine CEP because they are too far away from the original simulation points along the SU(3)-symmetric line.

Table II also lists the value of $\kappa_{1,E}$. To obtain them, we go back to the analysis in Fig. 2. We extrapolate κ_1 for the peak position linearly to the thermodynamic limit by $1/N_L^3$ for each β and κ_s . For given κ_s , we then fit the results as a quadratic function of β , and calculate $\kappa_{1,E}$ by setting $\beta = \beta_E$.

In Fig. 4, we plot $1/\kappa_{s,E}$ as a function of $1/\kappa_{1,E}$ by open circles; they represent our estimate of CEL. We also plot the points where we have performed zero temperature simulations to calculate the pseudo-scalar meson masses. We have generated $O(500)$ configurations at $\beta = 1.72$ on a $16^3 \times 32$ lattice for each (κ_1, κ_s) . The simulation parameters together with the Wilson flow scale $\sqrt{t_0}/a$ [22] and pseudo-scalar meson masses are summarized in Table III.

To calculate the pseudo scalar meson masses along CEL, a linear interpolation in Ward identity quark masses is

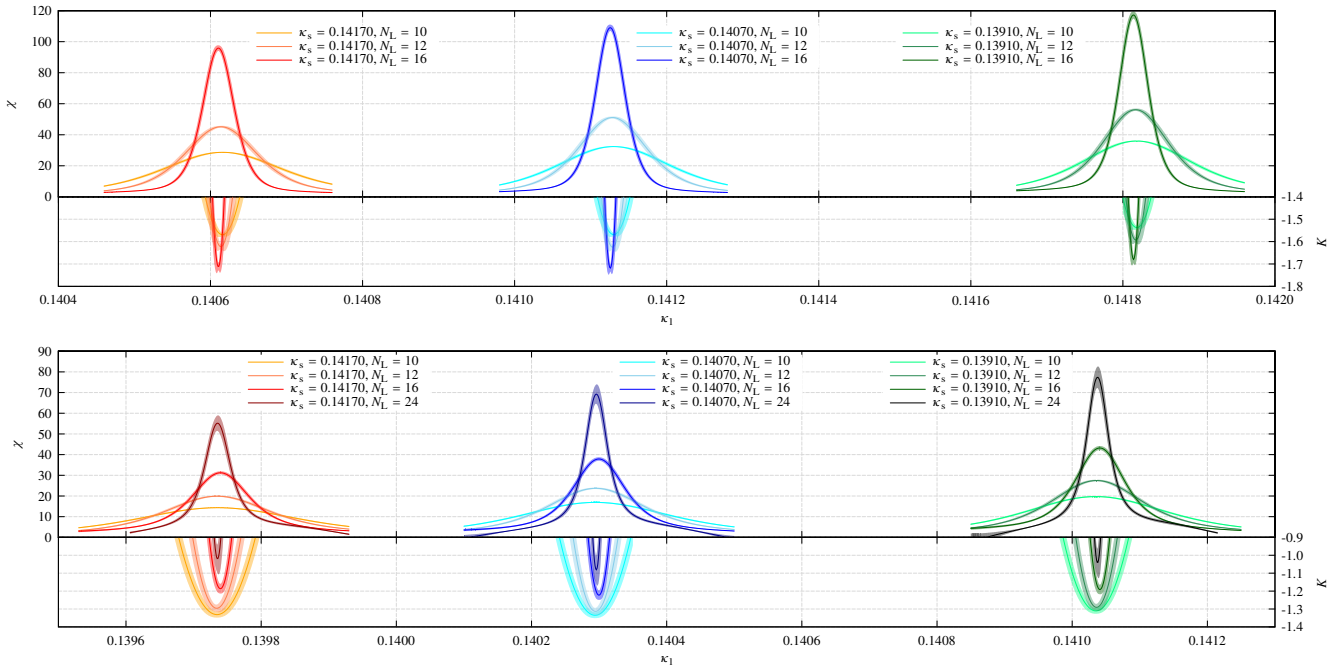


FIG. 2. χ and K for $\kappa_s = 0.13910, 0.14070, 0.14170$ as a function of κ_1 at $\beta = 1.715$ (upper) and 1.73 (lower).

sufficiently good in such a tiny parameter region. Thus, we perform a fit constrained by flavor symmetry of form,

$$\begin{aligned}
 (am_\pi)^2 &= 2A_1\bar{m}_l + 2A_2\bar{m}_s, \\
 (am_K)^2 &= (A_1 + A_3)\bar{m}_l + (A_2 + A_4)\bar{m}_s, \\
 (am_{\eta_s})^2 &= 2A_3\bar{m}_l + 2A_4\bar{m}_s, \\
 \sqrt{t_0}/a &= A_5 + 2A_6\bar{m}_l + A_6\bar{m}_s,
 \end{aligned} \tag{6}$$

with $\bar{m}_l = 1/\kappa_1 - 1/\kappa_0$, $\bar{m}_s = 1/\kappa_s - 1/\kappa_0$. We obtain $\kappa_0 = 0.1419248(25)$, $A_1 = 3.0896(55)$, $A_2 = 0.8494(37)$, $A_3 = 1.8091(54)$, $A_4 = 2.1228(38)$, $A_5 = 0.87742(43)$, $A_6 = -0.5034(20)$, and $\chi^2/\text{d.o.f.} = 16.9$.

Figure 5 shows the results for $(\sqrt{t_0}m_\pi)^2$ and $(\sqrt{t_0}m_{\eta_s})^2$ along CEL. We fit the data points by the following three polynomial functions up to fourth order in order to check higher order contributions against the second derivative.

$$\begin{aligned}
 f_2(x) &= b_{2,0} - 2(x - b_{2,0}) + b_{2,1}(x - b_{2,0})^2, \\
 f_3(x) &= b_{3,0} - 2(x - b_{3,0}) + b_{3,1}(x - b_{3,0})^2 + b_{3,2}(x - b_{3,0})^3, \\
 f_4(x) &= b_{4,0} - 2(x - b_{4,0}) + b_{4,1}(x - b_{4,0})^2 + b_{4,2}(x - b_{4,0})^3 + b_{4,3}(x - b_{4,0})^4,
 \end{aligned} \tag{7}$$

where $f(x) = (\sqrt{t_0}m_{\eta_s})^2$ and $x = (\sqrt{t_0}m_\pi)^2$. The fit results are given in Table IV. We find that the results are reasonably consistent with a slope of -2 and a positive second derivative at CEP.

IV. SUMMARY

We have investigated CEL of the finite temperature phase transition of QCD with non-perturbatively $O(a)$ -improved Wilson-clover fermion action around the $SU(3)$ -symmetric point at zero chemical potential and $N_T = 6$. Our method of kurtosis intersection point analysis aided by multi-parameter, multi-ensemble reweighting works well. As results, we could precisely determine CEL over a range $0.25 \leq (\sqrt{t_0}m_\pi)^2 \leq 0.35$ sandwiching the $SU(3)$ -symmetric point at $(\sqrt{t_0}m_\pi)^2 \approx 0.3$, and found -2 for the slope and a positive second derivative around m^{sym} on the Columbia plot.

We need to add to remarks on our results. First, for zero temperature simulations, we used a slightly different β than β_E . We think that this difference will not change our conclusion since it is only an effect of 0.3% or so in hadron mass values. Second, our study is conducted at just single lattice spacing of $a \approx 0.19$ fm. We are pursuing simulations with a larger N_T to obtain conclusive results, especially for the second derivative. Finally, the physical

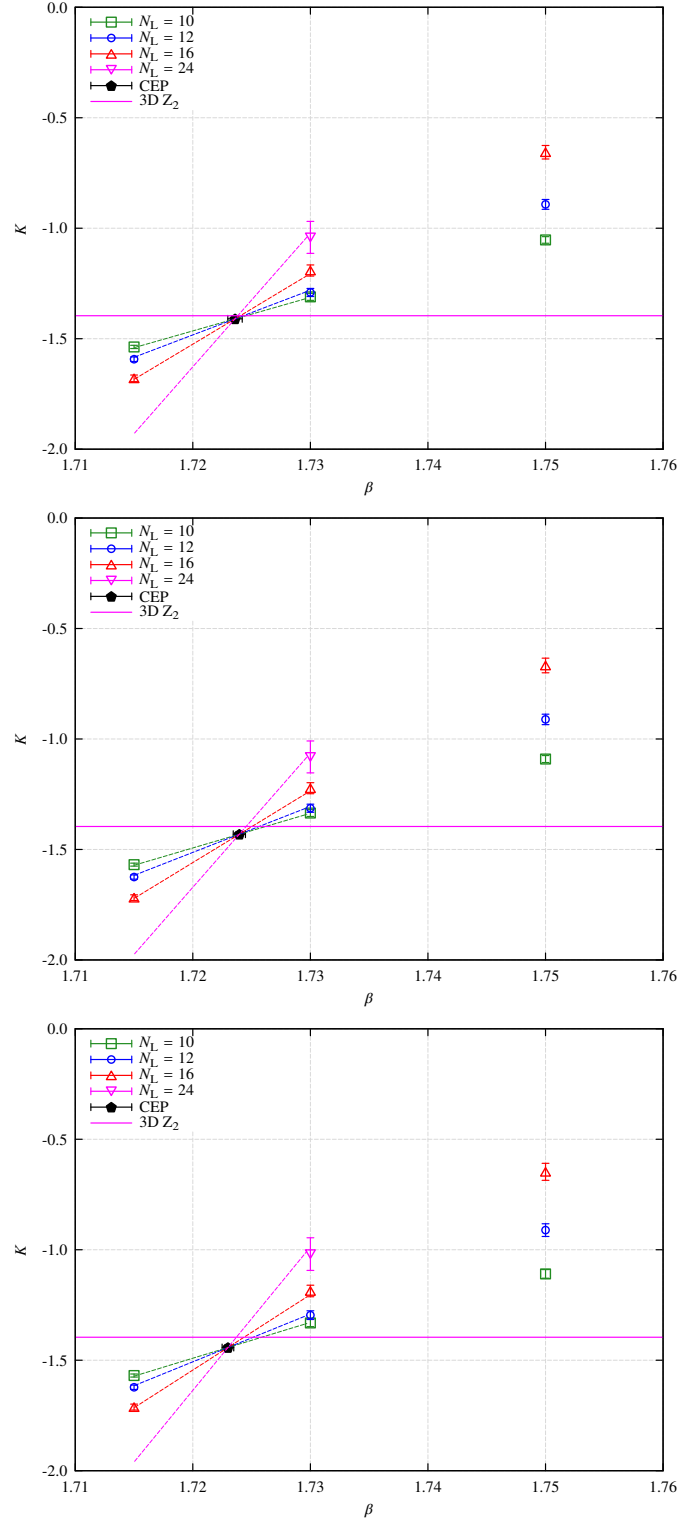


FIG. 3. Typical kurtosis intersection plots. These are for $\kappa_s = 0.13910$ (top), 0.14070 (middle) and 0.14170 (bottom).

point at $(\sqrt{t_0}m_\pi)^2 \approx 0.01$ is quite far from the $SU(3)$ -symmetric point. Thus, $N_f = 2 + 1$ simulations are needed to investigate CEL as it approaches the physical point.

TABLE II. Fitting results for eq. (5). $\kappa_{1,E}$ is obtained by interpolation to β_E after fitting with quadratic function of β (see text for more details). $\kappa_{s,E}$ has no error because we fix them as target parameters of the reweighing method.

$\kappa_{s,E}$	β_E	$\kappa_{1,E}$	K_E	ν	A	$\chi^2/\text{d.o.f.}$
0.13910	1.72359(61)	0.1413751(20)	-1.410(13)	0.633(46)	0.40(12)	0.58
0.13920	1.72364(60)	0.1413321(21)	-1.411(13)	0.635(46)	0.40(12)	0.57
0.13930	1.72370(60)	0.1412884(21)	-1.412(13)	0.637(45)	0.41(12)	0.55
0.13940	1.72376(59)	0.1412441(21)	-1.414(12)	0.638(45)	0.41(11)	0.54
0.13950	1.72381(58)	0.1411993(20)	-1.415(12)	0.639(44)	0.42(11)	0.53
0.13960	1.72386(57)	0.1411540(21)	-1.416(12)	0.641(44)	0.42(11)	0.51
0.13970	1.72391(57)	0.1411085(21)	-1.417(12)	0.642(43)	0.43(11)	0.50
0.13980	1.72395(56)	0.1410623(21)	-1.418(12)	0.643(43)	0.43(11)	0.49
0.13990	1.72398(56)	0.1410159(21)	-1.420(12)	0.644(42)	0.43(11)	0.49
0.14000	1.72401(56)	0.1409692(21)	-1.421(12)	0.645(42)	0.43(11)	0.48
0.14010	1.72404(55)	0.1409220(21)	-1.422(12)	0.645(42)	0.44(11)	0.48
0.14020	1.72405(55)	0.1408747(59)	-1.423(12)	0.646(42)	0.44(11)	0.48
0.14030	1.72406(55)	0.1408273(21)	-1.425(12)	0.646(42)	0.44(11)	0.47
0.14040	1.72405(54)	0.1407798(22)	-1.426(12)	0.646(41)	0.44(11)	0.47
0.14050	1.72403(53)	0.1407324(28)	-1.428(12)	0.646(41)	0.44(11)	0.46
0.14060	1.72400(53)	0.1406849(22)	-1.429(11)	0.647(40)	0.44(11)	0.45
0.14070	1.72396(52)	0.1406374(22)	-1.431(11)	0.647(39)	0.45(11)	0.43
0.14080	1.72390(51)	0.1405899(22)	-1.433(11)	0.646(39)	0.45(10)	0.43
0.14090	1.72384(50)	0.1405421(22)	-1.434(11)	0.646(38)	0.45(10)	0.42
0.14100	1.72376(49)	0.1404941(27)	-1.436(11)	0.645(38)	0.44(10)	0.42
0.14110	1.72368(49)	0.1404459(22)	-1.437(11)	0.643(38)	0.44(10)	0.42
0.14120	1.72359(49)	0.1403976(23)	-1.439(11)	0.641(38)	0.44(10)	0.43
0.14130	1.72349(49)	0.1403490(22)	-1.440(11)	0.639(38)	0.43(10)	0.44
0.14140	1.72338(49)	0.1403004(23)	-1.441(11)	0.636(38)	0.43(10)	0.45
0.14150	1.72326(50)	0.1402515(23)	-1.442(11)	0.633(38)	0.42(10)	0.47
0.14160	1.72312(50)	0.1402023(27)	-1.443(11)	0.631(38)	0.42(10)	0.48
0.14170	1.72299(49)	0.1401529(28)	-1.443(11)	0.631(38)	0.42(10)	0.47

ACKNOWLEDGMENTS

The BQCD code [16] was used in this work. This research used computational resources of HA-PACS and COMA provided by Interdisciplinary Computational Science Program in Center for Computational Sciences, University of Tsukuba, System E at Kyoto University through the HPCI System Research project (Project ID:hp140180) and PRIMERGY CX400 tatara at Kyushu University. This work is supported by JSPS KAKENHI Grant Numbers 23740177 and 26800130, FOCUS Establishing Supercomputing Center of Excellence and Kanazawa University SAKI-GAKE Project.

-
- [1] F. R. Brown *et al.*, Phys. Rev. Lett., **65**, 2491 (1990).
[2] R. D. Pisarski and F. Wilczek, Phys. Rev. D **29**, 338 (1984).
[3] S. Gavin, A. Gocksch and R. D. Pisarski, Phys. Rev. D **49**, 3079 (1994).
[4] S. Aoki *et al.* (JLQCD Collaboration), Nucl. Phys. Proc.Suppl. **73**, 459 (1999).
[5] F. Karsch, E. Laermann and C. Schmidt, Phys. Lett. B **520** 41 (2001), [arXiv:hep-lat/0107020].
[6] D. Smith and C. Schmidt, PoS(Lattice 2011), 216 (2011). [arXiv:1109.6729[hep-lat]]
[7] G. Endrődi *et al.*, PoS(Lattice 2007), 182 (2007), [arXiv:0710.0998 [hep-lat]].
[8] H.-T. Ding *et al.*, PoS(Lattice 2011), 191 (2011), [arXiv:1111.0185 [hep-lat]].
[9] Y. Iwasaki, K. Kanaya, S. Kaya, S. Sakai and T. Yoshié, Phys. Rev. D **54**, 7010 (1996), [arXiv:hep-lat/9605030]
[10] P. de Forcrand and O. Philipsen, JHEP **0701**, 077 (2007), [arXiv:hep-lat/0607017].

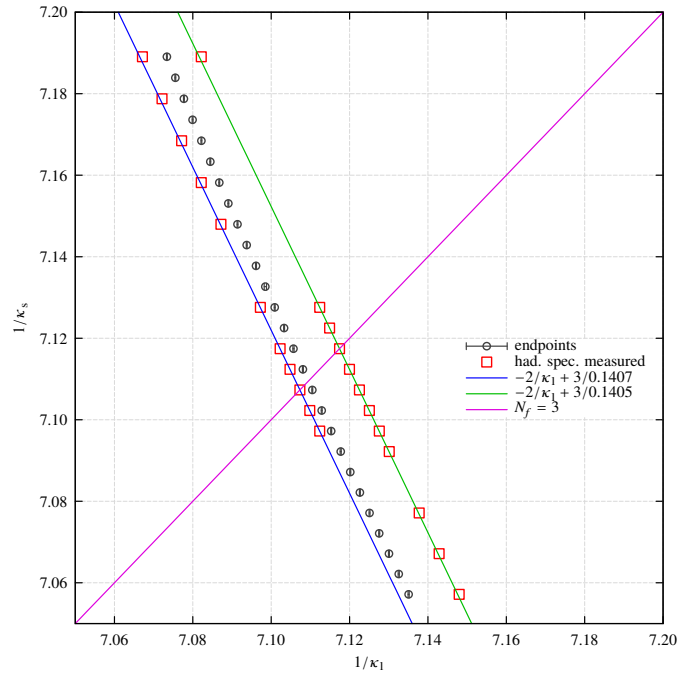


FIG. 4. Results for the critical endpoints in the plane of $1/\kappa_1$ and $1/\kappa_s$ (black open circles). Also shown (red squares) are the points where zero temperature simulations are carried out to calculate hadron masses. SU(3)-symmetric line is drawn in pink, while for green and blue lines the sum of three quark masses is constant.

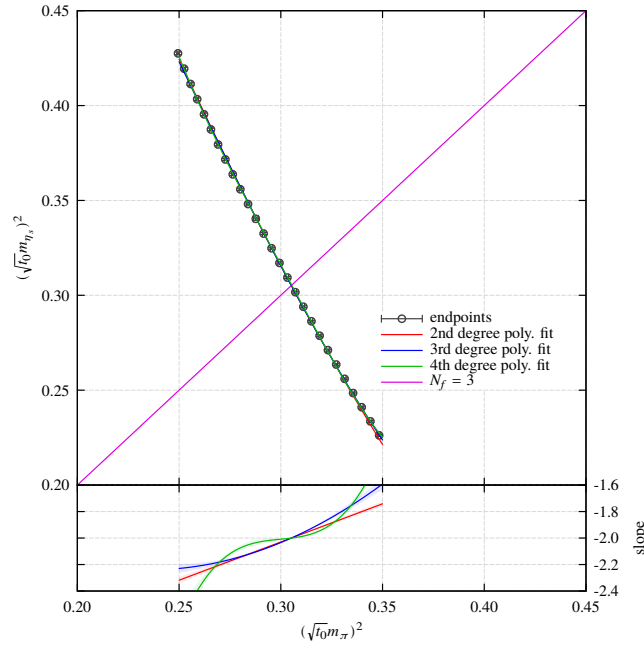


FIG. 5. CEL in the plane of $(\sqrt{t_0}m_\pi)^2$ and $(\sqrt{t_0}m_\eta)^2$ and the slope along CEL calculated by the fit in eq. (7). Pink line denotes the line of SU(3) symmetry ($N_f = 3$). Three types of polynomial fitting results are overlapping in upper plot.

- [11] X. -Y. Jin, Y. Kuramashi, Y. Nakamura, S. Takeda and A. Ukawa, Phys. Rev. D **91**, 014508 (2015) [arXiv:1411.7461 [hep-lat]].
- [12] K. Rajagopal, appearing in Quark-Gluon Plasma 2, edited by R. Hwa, World Scientific, 1995, [arXiv:hep-ph/9504310].
- [13] X. -Y. Jin, Y. Kuramashi, Y. Nakamura, S. Takeda and A. Ukawa, Phys. Rev. D **92**, 114511 (2015) [arXiv:1504.00113]

TABLE III. $\sqrt{t_0}/a$ and pseudo-scalar masses in lattice unit at $\beta = 1.72$ on $16^3 \times 32$

κ_1	κ_s	$\sqrt{t_0}/a$	am_π	am_K	am_{η_s}
0.140600	0.140900	0.78338(31)	0.7054(10)	0.6917(10)	0.6778(10)
0.140650	0.140800	0.78324(33)	0.7015(10)	0.6947(10)	0.6878(10)
0.140700	0.140700	0.78391(32)	0.6960(11)	0.6960(11)	0.6960(11)
0.140750	0.140600	0.78369(31)	0.6925(11)	0.6994(11)	0.7063(11)
0.140800	0.140500	0.78331(31)	0.6881(13)	0.7019(13)	0.7154(13)
0.140900	0.140300	0.78397(43)	0.6755(13)	0.7032(13)	0.7300(13)
0.141100	0.139900	0.78420(39)	0.6573(12)	0.7133(12)	0.7654(12)
0.141200	0.139700	0.78538(33)	0.6444(10)	0.7146(10)	0.7788(09)
0.141300	0.139500	0.78639(25)	0.6319(12)	0.7170(11)	0.7936(11)
0.141400	0.139300	0.78784(27)	0.6174(12)	0.7174(11)	0.8059(10)
0.141500	0.139100	0.78799(45)	0.6018(14)	0.7173(12)	0.8176(11)
0.139900	0.141700	0.77075(28)	0.7996(11)	0.7226(11)	0.6368(12)
0.140000	0.141500	0.77037(26)	0.7895(16)	0.7252(17)	0.6549(18)
0.140100	0.141300	0.77002(25)	0.7835(09)	0.7321(09)	0.6770(10)
0.140250	0.141000	0.76907(26)	0.7722(09)	0.7401(09)	0.7067(09)
0.140300	0.140900	0.76882(27)	0.7696(11)	0.7438(11)	0.7172(11)
0.140350	0.140800	0.76894(27)	0.7652(11)	0.7459(11)	0.7260(11)
0.140400	0.140700	0.76868(27)	0.7620(14)	0.7491(14)	0.7360(14)
0.140450	0.140600	0.76857(27)	0.7583(11)	0.7519(11)	0.7453(11)
0.140500	0.140500	0.76843(27)	0.7542(12)	0.7542(12)	0.7542(12)
0.140550	0.140400	0.76875(27)	0.7491(10)	0.7555(10)	0.7620(10)
0.140600	0.140300	0.76887(28)	0.7428(11)	0.7558(11)	0.7687(11)
0.141200	0.139100	0.77111(26)	0.6845(11)	0.7780(10)	0.8619(10)

TABLE IV. Results of polynomial fitting for CEL.

func.	b_0	b_1	b_2	b_3	$\chi^2/\text{d.o.f.}$
f_2	0.305194(83)	2.88(22)	—	—	1.619
f_3	0.305128(84)	3.44(26)	16.4(4.3)	—	1.039
f_4	0.30534(11)	0.96(71)	27.2(5.3)	1212(325)	0.481

[hep-lat]].

- [14] Y. Iwasaki, Report No. UTHEP-118 (1983), [arXiv:1111.7054].
[15] S. Aoki *et al.* (CP-PACS and JLQCD Collaborations), Phys. Rev. D **73**, 034501 (2006).
[16] Y. Nakamura and H. Stüben, PoS(Lattice 2010), 040 (2010), [arXiv:1011.0199 [hep-lat]].
[17] M. Hasenbusch, Phys. Lett. B **519**, 177 (2001); M. Hasenbusch and K. Jansen, Nucl. Phys. **B659**, 299 (2003).
[18] M. A. Clark and A. D. Kennedy, Phys. Rev. Lett. **98**, 051601 (2007), [arXiv:hep-lat/0608015].
[19] I. P. Omelyan, I. M. Mryglod and R. Folk, Phys. Rev. E **65**, 056706 (2002); Comput. Phys. Commun. **151**, 272 (2003).
[20] J. C. Sexton and D. H. Weingarten, Nucl. Phys. **B380**, 665 (1992).
[21] R. Brower, T. Ivanenko, A. Levi and K. Orginos, Nucl. Phys. **B484**, 353 (1997).
[22] M. Lüscher, JHEP **1008**, 071 (2010), [arXiv:1006.4518 [hep-lat]].